Low-energy $\alpha+{}^6$He elastic scattering with the resonating-group method

K. Fujimura,[1] D. Baye,[2] P. Descouvemont,[2] Y. Suzuki,[3] and K. Varga[4,*]
[1]*Graduate School of Science and Technology, Niigata University, Niigata 950-2181, Japan*
[2]*Physique Nucléaire Théorique et Physique Mathématique, C.P. 229, Université Libre de Bruxelles, B-1050 Brussels, Belgium*
[3]*Department of Physics, Niigata University, Niigata 950-2181, Japan*
[4]*RIKEN, Hirosawa, Wako, Saitama 351-0198, Japan*
(Received 17 August 1998)

The $\alpha+{}^6$He elastic scattering is investigated within a microscopic multicluster model, involving a realistic description of the ^{6}He halo nucleus. Phase shifts and elastic-scattering cross sections are calculated up to $E_{\text{c.m.}}=15$ MeV with two variants of the resonating-group method. The model gives rise to 1^- and 3^- molecular states near $E_{\text{c.m.}}=0.5$ MeV and $E_{\text{c.m.}}=3.7$ MeV, respectively. We suggest that the broad 3^- resonance should be observable by comparing elastic cross sections at different energies. We also evaluate the order of magnitude of the ^{6}He breakup cross section. [S0556-2813(99)03902-3]

PACS number(s): 25.60.Bx, 25.55.Ci, 21.60.Gx, 24.10.Ht

I. INTRODUCTION

Low-energy radioactive nuclear beams become available for elastic-scattering experiments. They provide new types of confrontations between theory and experiment. The development of low-energy ^{6}He beams is particularly interesting as it offers a new way of exploring halos. Until recently, halo properties were mostly studied in high-energy collisions [1,2] and in β-decay experiments [3]. At present ^{6}He is the only halo nucleus available in low-energy beams. It is the simplest nucleus exhibiting an anomalously large matter radius [4] indicating the existence of a neutron halo [5], i.e., of a region of space where loosely bound neutrons have a significant probability of presence at a large distance from the core nucleons. Because of its small number of nucleons, ^{6}He is also the best described halo nucleus, with accurate microscopic wave functions [6–10].

Cross sections for the low-energy $\alpha+{}^6$He collision have been measured at Dubna [11] and at Louvain-la-Neuve [12]. Several interesting physical effects are expected to be observed. Elastic transfer of the halo neutrons has been the object of a study at the c.m. energy of 60.4 MeV in Ref. [11]. In Ref. [12], measurements at the c.m. energies of 11.6 and 15.9 MeV are analyzed with the help of the nucleus-nucleus potential obtained in a double folding model [10], and also show evidence for elastic transfer. This potential displays an unusually long tail, extending beyond the standard range of nucleus-nucleus potentials, which is due to the slow decrease of the ^{6}He density distribution. At energies close to the Coulomb barrier, systems in the same mass range exhibit resonances which can be interpreted in terms of molecular states. They correspond to weakly overlaping nuclei which form a short-lived system exhibiting a rotational spectrum. In the $\alpha+{}^6$He case, the larger radius of ^{6}He might lead to a more extended nuclear molecule [13]. All these effects are related to the halo existence and might provide new information about its properties.

Several models are able to predict some of these properties. However, most of them ultimately rely on experiment for some parameters. The double-folding model of Ref. [10] neglects antisymmetrization between the colliding nuclei. It can help in analyzing experimental data but does not lead to accurate predictions about molecular resonances or about the parity dependence of the potential without some parameter fitting. On the contrary, the resonating-group method (RGM) [14,15] allows a study of $\alpha+{}^6$He scattering which is independent of experimental data and involves few model assumptions and parameters. The main advantages of this approach are that full antisymmetrization over the ten nucleons participating in the collision is exactly taken into account and that the angular momentum and parity good quantum numbers are treated exactly.

The present RGM study of the $\alpha+{}^6$He system only requires the following model assumptions. (i) The α particle is described by a single cluster wave function involving a chosen configuration for the four nucleons. (ii) The ^{6}He halo nucleus is described as a three cluster system involving the same α cluster wave function. This wave function has a complicated structure. A large r.m.s. radius of ^{6}He must in particular be obtained in order to allow a realistic description of the neutron halo. (iii) An effective nucleon-nucleon interaction giving good results for neighboring light systems is employed. The model is parameter-free as soon as this interaction is selected. These conditions can be met in two different ways. A multicluster model [16,17] including the ^{6}He wave function of Ref. [10] is in principle possible. In this model, all calculations are performed numerically and the collision matrices and scattering cross sections are easily calculated with the microscopic *R*-matrix method (MRM) [18,19]. However, the computing time would be very large because of the simultaneous projection on the ^{6}He total angular momentum and on the $\alpha+{}^6$He relative angular momentum. Another approach, which we adopt here, relies on the multicluster model developed in Refs. [7,8,20] and on a

*Permanent address: Physics Division, Argonne National Laboratory, 9700 South Cass Avenue, Argonne, IL 60439.

 ©1999 The American Physical Society

stochastic-variational ^{6}He wave function defined as in Ref. [9]. Here the angular momenta are fixed in the structure of the basis functions and analytical calculations are performed symbolically on a computer. The cross sections can be obtained either by adapting the MRM to the present basis states or by using the variational method [21].

The aim of the present work is to perform a calculation of the $\alpha+^6$He scattering in the RGM by using an accurate wave function for ^{6}He obtained with the Minnesota interaction [22]. This model should provide a quite realistic evaluation of the $\alpha+^6$He phase shifts and cross sections. These results give information about the existence of molecular resonances. In Sec. II, the ^{6}He internal wave function and the RGM scattering wave functions are described. Two methods for calculating the collision matrices from which the cross sections can be deduced are also presented. In Sec. III, results are described and discussed. Concluding remarks and perspectives are presented in Sec. IV.

II. THE MODEL

A. ^{6}He wave functions

As mentioned in the Introduction, we describe the ^{6}He nucleus as a three-cluster system $\alpha+n+n$ with the α cluster composed of four nucleons. This model has been used by many authors (see Refs. [8,23] for the detailed description of our microscopic model). We build up a trial function for ^{6}He as a sum of two cluster arrangements, $\mu_1=\alpha(nn)$ called a T type, and $\mu_2=(\alpha n)n$ called a Y type. These arrangements are suited to describe $\alpha+$dineutron-like and ^{5}He$+n$ configurations, respectvely.

The wave function of ^{6}He is given as a combination of the two arrangements and of the intercluster angular momenta:

$$\phi(^6\mathrm{He})=\sum_{\mu}\sum_{(l_1,l_2)L}\mathcal{A}\{\phi(\alpha)[\chi^{\mu}_{(l_1,l_2)L}(\boldsymbol{\rho}_1^{\mu},\boldsymbol{\rho}_2^{\mu})]\times\eta_L\}_{00}\}, \tag{1}$$

where $\mathcal{A}$ is the antisymmetrization operator, $\phi(\alpha)$ is the α-particle wave function, and $\chi^{\mu}_{(l_1,l_2)LM}(\boldsymbol{\rho}_1^{\mu},\boldsymbol{\rho}_2^{\mu})$ is the intercluster relative function depending on the intercluster Jacobi coordinates, $\boldsymbol{\rho}_1^{\mu}$ and $\boldsymbol{\rho}_2^{\mu}$, in the arrangement μ. The partial waves l_1,l_2 are coupled to the total orbital angular momentum L, and η_{SM} is the spin function of the two halo neutrons. The spin S is chosen to be equal to L to get the total angular momentum zero for ^{6}He. The values (l_1,l_2,L) included in the calculation are given in [8,23], that is, $(l_1,l_2,L)=(1,1,1),(0,0,0)$ for the T type and $(l_1,l_2,L)=(1,1,0),(1,1,1)$ for the Y type.

The intercluster relative motion function is obtained in Gaussian (nodeless harmonic-oscillator function) expansions

$$\chi^{\mu}_{(l_1,l_2)LM}(\boldsymbol{\rho}_1,\boldsymbol{\rho}_2)=\sum_{\nu_1,\nu_2}c(\nu_1,\nu_2)[\Gamma_{l_1m_1}(\nu_1,\boldsymbol{\rho}_1)\times\Gamma_{l_2m_2}(\nu_2,\boldsymbol{\rho}_2)]_{LM}, \tag{2}$$

where

$$\Gamma_{lm}(\nu,\boldsymbol{\rho})=\left[\frac{2^{2l+7/2}\nu^{l+3/2}}{\sqrt{\pi}(2l+1)!!}\right]^{1/2}\rho^l\exp(-\nu\rho^2)Y_{lm}(\hat{\boldsymbol{\rho}})=\gamma_l(\nu,\rho)Y_{lm}(\hat{\boldsymbol{\rho}}). \tag{3}$$

B. $\alpha+^6$He wave functions

The $\alpha+^6$He wave function with angular momentum l and projection m can be expressed as

$$\Psi_{lm}=\sum_i\mathcal{A}\{\phi(\alpha)\phi_i(^6\mathrm{He})g_i^l(\rho)Y_{lm}(\hat{\boldsymbol{\rho}})\}, \tag{4}$$

where $\boldsymbol{\rho}=(\rho,\hat{\boldsymbol{\rho}})$ is the relative coordinate between α and ^{6}He, and $\phi_i(^6\mathrm{He})$ is the intrinsic wave function of ^{6}He in excitation level i, which was obtained in the previous subsection.

In the RGM treatment of scattering, the intrinsic wave functions of the α and ^{6}He clusters are kept fixed, though the ^{6}He cluster is allowed to be excited into the pseudostates. On the contrary, the relative function $g_i^l(\rho)$ has to be determined under proper boundary conditions. In the asymptotic region, where the nuclear interaction between α and ^{6}He vanishes, the function $g_i^l(\rho)$ can be expressed in terms of Coulomb functions. Thus we only need to give a prescription of how $g_i(\rho)$ can be described accurately in the internal region. There are two widely used basis functions: one is the shifted Gaussian function and the other is the tempered Gaussian function (3). We use the latter basis in the present study because all the needed matrix elements are tailored in that basis.

The function $g_i^l(\rho)$ is expanded as follows:

$$g_i^l(\rho)=\sum_n f_{in}^l\,\gamma_l(\nu_n,\rho). \tag{5}$$

Here the ν_n values characterize the falloff of the Gaussians, so that they have to be chosen flexibly enough to be able to approximate the wave function in the internal region. More details are given in Sec. III.

Let us define the following matrix elements, evaluated over the whole space:

$$\begin{Bmatrix} H_{ij}^l(\nu,\nu') \\ N_{ij}^l(\nu,\nu') \\ \mathcal{L}_{ij}^l(\nu,\nu') \end{Bmatrix}=\langle\mathcal{A}\{\phi(\alpha)\phi_i(^6\mathrm{He})\Gamma_{lm}(\nu,\boldsymbol{\rho})\}|\begin{Bmatrix} H \\ 1 \\ \mathcal{L} \end{Bmatrix}|\mathcal{A}\{\phi(\alpha)\phi_j(^6\mathrm{He})\Gamma_{lm}(\nu',\boldsymbol{\rho})\}\rangle, \tag{6}$$

where H is the microscopic ten-body Hamiltonian, and $\mathcal{L}$ is the Bloch operator [18], which will be used later. As the ^{6}He nucleus is described with an $\alpha+n+n$ three-cluster model, the above matrix elements are evaluated in a $\alpha+\alpha+n+n$ four-cluster model. This microscopic four-cluster description has recently been applied to the spectroscopic study of ^{10}Be [24] and the method of calculating the matrix element is available.

In fact we need matrix elements such that the integration over the relative coordinate is limited to the internal region only. In the Appendix we show how the external part of the matrix element is subtracted from the one calculated over the entire space.

C. *R*-matrix and variational methods

The $\alpha+^6$He phase shifts are determined in two ways: the microscopic *R*-matrix method (MRM, see Ref. [18]), and the variational method (VM, see Ref. [21]). In both methods, the configuration space is divided in two regions: the internal region (of radius a) where the antisymmetrization and the nuclear interaction between the clusters must be taken into account, and the external region, where they are negligible. In the internal region, the total wave function is given by Eq. (4), whereas it is assumed to reach its asymptotic behavior in the external region.

Let us start with the MRM. In the present model, the relative wave function is expanded in the internal region as

$$g_i^l(\rho)=\sum_n f_{in}^l\,\gamma_l(\nu_n,\rho), \tag{7}$$

and in the external region as

$$g_i^l(\rho)=\begin{cases} i^{l+1}[\pi(2l+1)/v]^{1/2}[I_l(k_i,\rho)\,\delta_{i1}-U_{1i}^l O_l(k_i,\rho)]/k_i\rho & \text{for open channels} \\ A_i^l\,W_l^{(+)}(k_i,\rho)/k_i\rho & \text{for closed channels,} \end{cases} \tag{8}$$

where k_i is the wave number in channel i, v is the relative velocity in the entrance channel 1, I_l and O_l are the ingoing and outgoing Coulomb functions, and $W_l^{(+)}$ is the Whittaker function. Coefficients A_i^l are the amplitudes of closed-channel wave functions, and U^l is the collision matrix. We refer the reader to Ref. [25] for details.

The MRM has been widely described with shifted Gaussian functions [18,25]. With tempered Gaussians, it is easily shown that the collision matrix at energy E can be deduced from the R matrix

$$R_{ij}^l(E)=\frac{\hbar^2 a}{2\mu}\sum_{nn}\,\gamma_l(\nu_n,a)\,(C^l)^{-1}_{in,jn'}\,\gamma_l(\nu_n',a). \tag{9}$$

The calculation of matrix $C^l(E)$ requires the matrix elements of the Hamiltonian over the internal region only. Such matrix elements, denoted as $\tilde{H}_{ij}^l(\nu,\nu')$ for the Hamiltonian, and $\tilde{N}_{ij}^l(\nu,\nu')$ for the overlap, are obtained in two steps: a calculation over the whole space, and a correction over the external region. This calculation is outlined in the Appendix. Let us point out here that matrix $\tilde{H}$ is not symmetric because of the nonhermiticity of the kinetic energy operator in a finite region of space. As explained in Ref. [18], matrix $C^l(E)$ reads

$$C_{in,jn'}^l=\tilde{H}_{ij}^l(\nu_n,\nu_n')+\mathcal{L}_{ij}^l(\nu_n,\nu_n')-E\tilde{N}_{ij}^l(\nu_n,\nu_n'), \tag{10}$$

which is symmetric owing to the Bloch operator.

Let us define the Z^l matrix as

$$Z_{ij}^l=I_l(k_i,a)\,\delta_{ij}-ak_jR_{ij}^lI_l'(k_j,a), \tag{11}$$

which yields the collision matrix [18]

$$U_{ij}^l=\sum_k\,(Z^{l\star})^{-1}_{ik}\,Z_{kj}^l. \tag{12}$$

In the MRM, the collision matrix is easily shown to be symmetric and unitary for any choice of the channel radius. The stability of the collision matrix with respect to a provides a strong test on the numerical accuracy of the method.

In the present study, the phase shifts are nearly independent of the channel radius up to about 15 MeV. The choice of the channel radius results from a compromise between the requirements of the *R*-matrix method (antisymmetrization and nuclear interaction must be negligible), and the ability of the basis to simulate a scattering wave function up to this channel radius. The halo structure of the ^{6}He ground state, and the large radius of some pseudostates require the channel radius to be at least 10 fm. The choice of the basis parameters ν_n must be carefully done in order to have some flexibility of the wave function at the channel radius, without introducing numerical redundancy. In this respect, the shifted Gaussian basis is more convenient for collision studies. Anyway the stability of the phase shifts is of the order of 1° or less for energies up to 13 MeV, and for channel radii of 10 and 11 fm.

In parallel with the MRM, we have used the VM (see Sec. 2.4 of Ref. [21]), where the scattering wave function and the collision matrix are determined from the variational principle

$$\delta\langle\tilde{\Psi}_{lm}|H-E|\Psi_{lm}\rangle=0, \tag{13}$$

where $\tilde{\Psi}_{lm}$ is the time reversal of Ψ_{lm}. The relative function $g_i^l(\rho)$ in the internal region is approximated by combinations of Gaussians as follows:

$$g_i^l(\rho)=\sum_n f_{in}^l \chi_{in}(\rho), \tag{14}$$

where

$$\chi_{in}(\rho)=\begin{cases}\alpha_{in}\gamma_l(\nu_n,\rho) & \text{for } \rho\leqslant a\\ \chi_i^{(-)}(k_i,\rho)-s_{in}\chi_i^{(+)}(k_i,\rho) & \text{for } \rho>a,\end{cases} \tag{15}$$

and

$$\chi_i^{(\pm)}(k_i,\rho)=\begin{cases}[G_l(k_i,\rho)\pm iF_l(k_i,\rho)]\exp(\mp i\sigma_{li})/\sqrt{v}\rho & \text{for open channels}\\ W_l^{(\pm)}(k_i,\rho)/\rho & \text{for closed channels,}\end{cases} \tag{16}$$

with the condition

$$\sum_n f_{in}^l=\delta_{i1}. \tag{17}$$

Here F_l and G_l are the regular and irregular Coulomb functions, $W_l^{(+)}$ and $W_l^{(-)}$ are the damping and diverging Whittaker functions, respectively, and σ_{li} is the Coulomb phase shift.

The values of α_{in} and s_{in} are determined by the condition that the function $\chi_{in}(\rho)$ is smooth at the channel radius a. The set of values f_{in}^l are variational parameters, and are determined from Eq. (13). Using Eq. (17), Eq. (14) can be written as

$$g_i^l(\rho)=\chi_{in_0}(\rho)\delta_{i1}+\sum_{n\neq n_0} f_{in}^l[\chi_{in}(\rho)-\chi_{in_0}(\rho)]. \tag{18}$$

The collision matrix can be expressed as follows:

$$U_{i1}^l=\sum_n f_{in}^l s_{in}+\frac{i}{\hbar}\left[\sum_n\sum_k (\mathcal{K})_{in_0,kn} f_{kn}^l\right], \tag{19}$$

where the matrix $\mathcal{K}^l$ is deduced from

$$\mathcal{K}_{in_0,kn}^l=\alpha_{in_0}\alpha_{kn}[\tilde{H}_{ij}^l(\nu_{n_0},\nu_n)-E\tilde{N}_{ij}^l(\nu_{n_0},\nu_n)]. \tag{20}$$

Here n_0 can be taken arbitrarily [21]. The correction due to the external region can be made in exactly the same way as in the R matrix. Notice that the collision matrix is symmetric but not unitary. This property is only fulfilled when the numerical accuracy of the calculation is sufficient, and therefore also provides a strong test of the calculation.

In the energy range of interest, the phase shifts calculated with $a=10$ fm and $a=11$ fm do not differ by more than 0.5°, and unitarity is verified within 3% at most. The VM and MRM methods, although based on rather different approaches, provide phase shifts agreeing within 2° or less below 15 MeV. This consistency test is very important in the present work where, for the first time, we are using halo wave functions in a microscopic study of a nucleus-nucleus collision. Special attention must be paid to the numerical conditions, and the agreement between the MRM and VM methods gives us confidence about the numerical results.

III. RESULTS

A. Conditions of the calculations

We use the Minnesota potential [22], with parameter $u=0.95$, as recommended in the RGM study of $\alpha+\alpha$ scattering. The spin-orbit potential was taken as in Ref. [24]. The intrinsic wave function $\phi(\alpha)$ of the α cluster is constructed from a harmonic-oscillator Slater determinant with size parameter ν, which is taken as 0.26 fm^{-2} to reproduce the experimental value of its charge radius.

For the ^{6}He wave functions, a set of nonlinear parameters, ν_1 and ν_2 [see Eq. (2)], characterizes the basis element in the variational calculation. The basis size is increased one by one and each new element is chosen by a stochastic selection, that is, the best candidate among a number of random trials is included in the basis set. The number of basis functions is kept as small as possible because otherwise the computational load for the calculation of $\alpha+^6$He matrix elements would be extremely expensive.

The basis dimension for ^{6}He is 15. Table I lists the first five energies and the corresponding radii. The lowest energy corresponds to the ground-state energy of ^{6}He. Compared to the experimental value, the calculated binding energy is by 400 keV too small. The root-mean-square radius of the lowest state is in good agreement with the empirical value determined from the analysis of the interaction cross-section measurement. The energies of other states are above the three-particle threshold since the ^{6}He nucleus, as a Borromean system, has no bound excited states. The positive-energy states are considered to be pseudostates which appear because no proper boundary condition is met in the asymptotics. We include these pseudostates in the $\alpha+^6$He scattering calculation since they are expected to simulate breakup

TABLE I. The energies (E) and the root-mean-square radii (R) of the lowest five states of ^{6}He obtained in a 15-dimension basis. Energies are from the $\alpha+n+n$ threshold.

Level	E (MeV)	R (fm)
1	−0.58	2.16
2	5.28	2.50
3	10.82	2.69
4	17.04	2.50
5	32.50	2.49

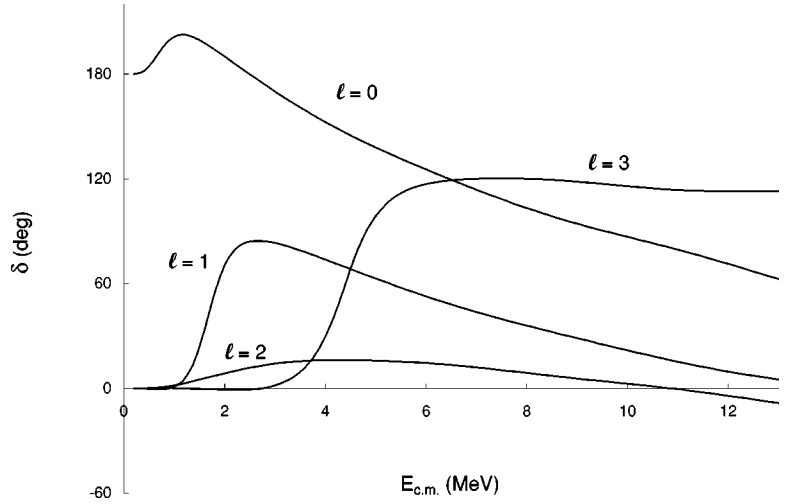

FIG. 1. Single channel $\alpha+^6$He phase shifts for $l=0$ to 3.

effects of ^{6}He into the 0^+ continuum.

The ν_n values [see Eq. (3)] in the $\alpha+^6$He relative motion are parametrized in a geometric progression:

$$\frac{1}{\sqrt{\nu_n}}=0.877\times 1.257^{n-1}(\text{fm}) \quad (n=1,2,\ldots,15). \quad (21)$$

This set of basis functions gives a good compromise between two requirements. The basis functions must be different enough to avoid numerical redundancy, but, for scattering studies, they must be flexible enough to simulate an oscillating behavior of the wave functions. After many trials, this choice turns out to be well adapted to the problem.

B. Elastic phase shifts

We present in Fig. 1 the $\alpha+^6$He elastic phase shifts in the single-channel approximation. Partial waves up to $l=3$ are considered. The positive-parity phase shifts present a very broad resonant structure near the Coulomb barrier. As shown in Table II, these partial waves contain one bound state. The 0^+ bound state approximates the ^{10}Be ground state. The present microscopic model underestimates the experimental [26] binding energy (-7.41 MeV), but the experimental 2^+-0^+ energy difference (3.37 MeV) is fairly well reproduced (3.43 MeV). The negative-parity phase shifts present a resonant behavior near 1.7 and 4.4 MeV for $l=1$ and $l=3$, respectively. The dimensionless reduced widths at a channel radius of 6 fm are $\theta_\alpha^2=23\%$ for $l=1$ and $\theta_\alpha^2=24\%$ for $l=3$. These large values are characteristic of molecular states, well known in other systems, such as $\alpha+\alpha$ [27], $\alpha+^{14}$C [28] or $\alpha+^{16}$O [29]. The possibility of observing the 3^- molecular state in elastic-scattering experiments will be discussed in the next subsection.

TABLE II. Energies and widths (in MeV) of ^{10}Be states.

J^π	E	Γ_α	E_{exp}
Single channel			
0^+	-4.13		-7.41
	0.7	≈ 0.7	-1.23
1^-	1.7	0.5	
2^+	-0.70		-4.04
3^-	4.4	0.8	
Multichannel			
0^+	-6.12		-7.41
	0.75	0.41	-1.23
	4.66	3.2×10^{-3}	
1^-	0.47	0.01	
2^+	-2.46		-4.04
	6.88	1.0×10^{-3}	
3^-	3.7	0.7	

These molecular resonances are of a different nature from the known 1^- and 3^- states of ^{10}Be at 5.96 and 7.37 MeV, respectively. Indeed, the wave functions (4) are characteristic of a negative-parity $K=0^-$ band. On the contrary, the known states belong, together with a 2^- state at 6.26 MeV, to a $K=1^-$ band. This band is expected in the SU(3) model [30] for the $(\lambda\mu)=(51)$ configuration which yields a $K=1^-$ band with 1^- to 6^- states.

In Fig. 2 we show the phase shifts obtained in the multichannel approach, i.e., with all ^{6}He pseudostates (15) included in the basis. Bound-state and resonance properties are gathered in Table II. As expected, $\alpha+^6$He states are lower than in the single-channel model. The energy and width of the 3^- molecular resonance are, however, weakly modified by the inclusion of $\alpha+^6$He* channels. The multichannel approach gives rise to additional resonances in the $l=0$ and $l=2$ partial waves ($E_{\text{c.m.}}=4.66$ and 6.88 MeV, respectively). These states have a dominant $\alpha+^6$He* structure and their energies are dependent on the threshold energies. They correspond to narrow resonances in the elastic channel.

C. Molecular states

The present model suggests the existence of $\alpha+^6$He molecular states near the Coulomb barrier. More especially, a 3^- state is a good candidate for such a structure. Using 3 MeV as the energy difference between the 1^- and 3^- states of the same $K=0^-$ band yields a mean distance of 5.4 fm between α and ^{6}He. This value is much larger than the sum of the nuclear radii, and supports the picture of a molecular

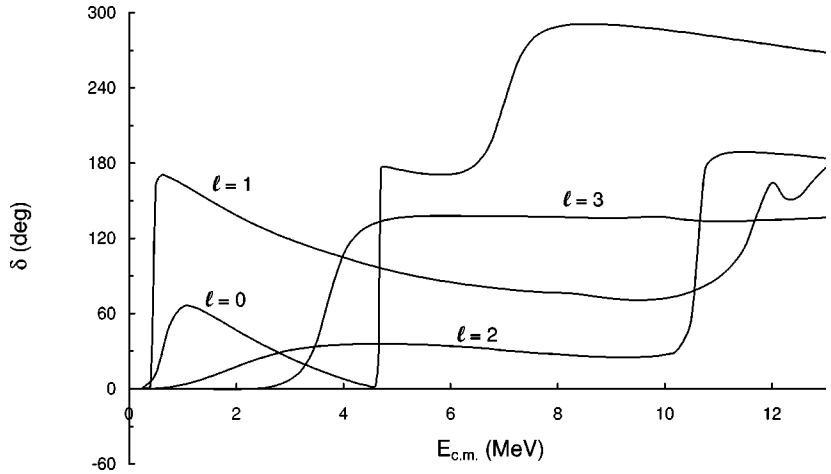

FIG. 2. Real parts of the multichannel $\alpha+{}^6$He phase shifts δ^l_{11} for $l=0$ to 3, obtained from $U^l_{11}=\exp(2i\delta^l_{11})$.

state. As shown in Fig. 3, evidence for the 3^- molecular state can be established from the differential elastic cross section, i.e., from experiments which can be realized with the radioactive beam facility of Louvain-la-Neuve. In this figure, we select the theoretical resonance energy 3.7 MeV (we consider the multichannel model), and two off-resonance energies, 1 MeV below and above the resonance. Partial waves up to $l=3$ are included. To test the convergence with respect to angular momentum, we have used a potential model [10] which nearly reproduces the microscopic phase shifts at low energies, to simulate higher-order phase shifts. The cross section at 3.7 MeV obtained by including partial waves up to $l=8$ is shown as a dotted line in Fig. 3. The differences with respect to the purely microscopic calculation performed with $l_{\max}=3$ are very small.

Figure 3 shows that, below the 3^- energy, the cross section is a smooth function, whereas it presents important oscillations at the resonance. The minima remain observable beyond the resonance energy. Of course the model is not expected to give this energy with high accuracy. However, molecular resonances are well established in many other systems, and are in general located close to the Coulomb barrier. We therefore believe that such a state should also exist in the $\alpha+{}^6$He scattering near $E_{\text{c.m.}}\approx 3-4$ MeV and should be observable in elastic-scattering cross sections. An experimental candidate for an $\alpha+{}^6$He molecular state has been observed by Soić *et al.* [13] at $E_{\text{c.m.}}=2.8$ MeV with a width of the order of 400 keV. This state is assigned by Soić *et al.* to $J=4^+$, on the basis of the similarity with an angular distribution measured by Hamada *et al.* [31] at $E_{\text{c.m.}}=4.4$ MeV. However, distorted-wave-Born-approximation fits are rather poor [31], and other spin assignments cannot be ruled out. In addition, the measured width of 400 keV corresponds to a dimensionless reduced width of 26% or 75% assuming $l=3$ or $l=4$, respectively (the channel radius is 6 fm). The present 3^- resonance at $E_{\text{c.m.}}=3.7$ MeV has a reduced width of 27% and, in spite of the energy difference (≈ 1 MeV), an assignment to the 2.8 MeV resonance observed by Soić *et al.* cannot be ruled out.

In Fig. 4, we present the total transfer cross section from the elastic channel to all $\alpha+{}^6$He* channels. This cross section is expected to simulate the breakup cross section of ^{6}He on α. Since the first pseudostate is located at 5.9 MeV, i.e.,

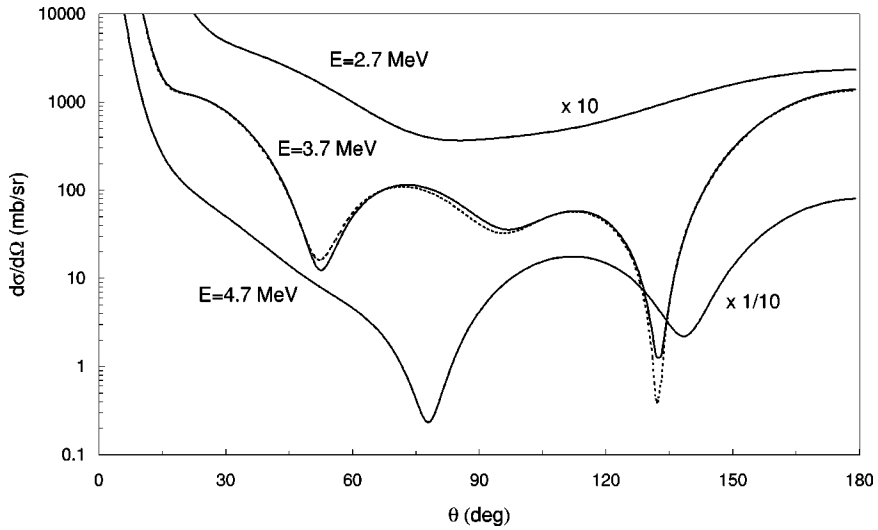

FIG. 3. Elastic cross sections on resonance (3.7 MeV) and off resonance ($l_{\max}=3$). The dotted line corresponds to a microscopic calculation for $l=0$ to 3, complemented by a potential model calculation for $l=4$ to 8.

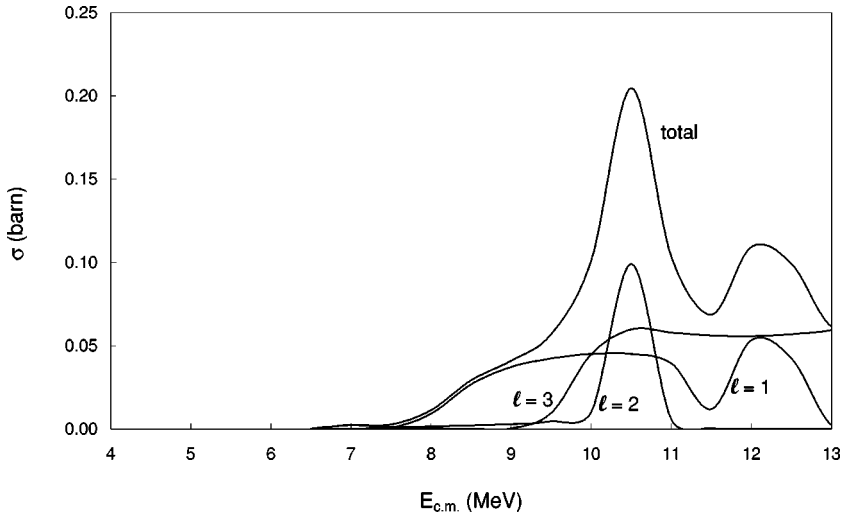

FIG. 4. $\alpha+^6$He breakup cross section. Contributions of partial waves are shown individually (the $l=0$ contribution is negligible at the scale of the figure).

much higher than the breakup threshold (0.98 MeV), the microscopic cross section must be considered as qualitative only. Two peaks are observed beyond 10 MeV, and are due to the $l=1$ and $l=2$ partial waves. The averaged amplitude is about 50 mb. Of course, other components where ^{6}He is excited into other states are also possible, but are not included here. Our value should therefore be considered as a lower limit.

D. Potential-model approximation

In order to interpret the microscopic results, we have used the $\alpha+^6$He potential of Ref. [10]. This potential [see Eq. (28) of Ref. [10]] contains a short-range term, obtained from a folding procedure of the Minnesota interaction with microscopic densities of α and ^{6}He, and a long-range term which accounts for the anomalously large r.m.s. radius of ^{6}He.

We have renormalized the short-range part in order to fit the present $\alpha+^6$He single-channel phase shifts. The renormalization factors are 1.4, 0.6, 1.2, and 0.75 for $l=0$ to 3, and clearly show that a parity effect must be introduced. This conclusion is supported by the recent elastic-scattering experiment of Raabe *et al.* [12]. The phase shifts obtained in this way are presented in Fig. 5, and are fairly close to the original RGM phase shifts. Without renormalization (dashed lines in Fig. 5), i.e., without any parity effect, the resonance properties cannot match the microscopic results.

IV. CONCLUSION

In this paper, we have investigated the $\alpha+^6$He elastic scattering at low energies in a purely microscopic model without a free parameter. The ^{6}He ground-state wave function provides a realistic description of its halo properties, i.e., a low binding energy, and an extended r.m.s. radius. Using this wave function in $\alpha+^6$He scattering is expected to give a fair description of the low-energy phase shifts and cross sections.

The model space has of course to be limited owing to the very high computer times needed. Only $J=0^+$ states of ^{6}He are included, but a 2^+ state which is known just above the $\alpha+n+n$ threshold as well as dipole excitations, might be

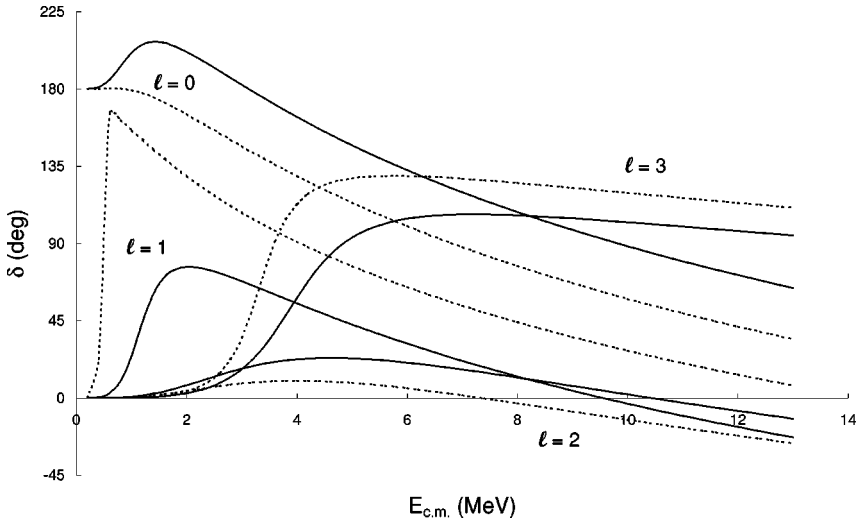

FIG. 5. $\alpha+^6$He phase shifts obtained in the potential model with renormalization (solid lines) and without renormalization (dashed lines).

considered. On the other hand, the relative angular momentum between α and ^{6}He is limited to $l_{\max}=3$. This reduces the energy range where cross sections can be calculated with precision.

The model has been tested through the ^{10}Be spectrum, which is in reasonable agreement with experiment in view of the restricted ten-nucleon space. The phase shifts present resonances in the 1^- and 3^- partial waves, which are considered as molecular states since they imply a large distance between the α and ^{6}He nuclei. We have shown the influence of the 3^- resonance in elastic cross sections, and suggested that it might be observable in future experiments using low-energy radioactive beams.

ACKNOWLEDGMENTS

We thank Y. Fujiwara for providing us the variational code. This work was supported in part by Grants-in-Aid for International Scientific Research (Joint Research) (No. 08044065) and for Scientific Research (No. 10640255) of the Ministry of Education, Science and Culture. This text presents research results of the Belgian program on interuniversity attraction poles initiated by the Belgian-state Federal Services for Scientific, Technical and Cultural Affairs. P.D. acknowledges the support of the National Fund for Scientific Research (FNRS), Belgium. D.B. and P.D. thank the FNRS for travel grants.

APPENDIX

In this Appendix, we evaluate matrix elements of the Hamiltonian in the external region. This correction is then subtracted from matrix elements calculated over the whole space $H^l_{ij}(\nu,\nu')$ and $N^l_{ij}(\nu,\nu')$ [Eq. (6)], and yields matrix elements $\tilde{H}^l_{ij}(\nu,\nu')$ and $\tilde{N}^l_{ij}(\nu,\nu')$ used in the MRM and in the VM.

When antisymmetrization between the colliding nuclei is negligible, this correction reduces to the evaluation of one-dimensional integrals. For example, one has in the MRM

$$\begin{aligned}
&\langle \phi(\alpha)\phi_i(^6\mathrm{He})\Gamma_{lm}(\nu,\boldsymbol{\rho})|H+\mathcal{L}|\phi(\alpha)\phi_j(^6\mathrm{He})\Gamma_{lm}(\nu',\boldsymbol{\rho})\rangle_E \\
&\quad=\delta_{ij}\int_a^\infty\left\{\frac{\hbar^2}{2\mu}\left[\frac{d}{d\rho}(\rho\gamma_l(\nu,\rho))\frac{d}{d\rho}(\rho\gamma_l(\nu',\rho))\right.\right. \\
&\qquad\left.+l(l+1)\gamma_l(\nu,\rho)\gamma_l(\nu',\rho)\right] \\
&\qquad\left.+4e^2\rho\gamma_l(\nu,\rho)\gamma_l(\nu',\rho)\right\}d\rho \\
&\quad=\delta_{ij}\left[\frac{\hbar^2}{2\mu}[4\nu\nu' J^l_4(x)-2(l+1)(\nu+\nu')J^l_2(x)\right. \\
&\qquad\left.+(l+1)(2l+1)J^l_0(x)]+4e^2J^l_1(x)\right],
\end{aligned} \tag{A1}$$

where $x=(\nu+\nu')a^2$, and the function $J^l_k(x)$ is defined as

$$\begin{aligned}
J^l_k(x)&=\int_a^\infty \rho^k\,\gamma_l(\nu,\rho)\gamma_l(\nu',\rho)\,d\rho \\
&=\sqrt{\frac{2(\nu\nu')^{l+3/2}}{\pi(\nu+\nu')^{2l+k+1}}}\frac{2^{2l+2}}{(2l+1)!!}\Gamma\left(l+\frac{k+1}{2},x\right),
\end{aligned} \tag{A2}$$

which involves the incomplete gamma function $\Gamma(n,x)$. The overlap is obtained from

$$\begin{aligned}
&\langle \phi(\alpha)\phi_i(^6\mathrm{He})\Gamma_{lm}(\nu,\boldsymbol{\rho})|\phi(\alpha)\phi_j(^6\mathrm{He})\Gamma_{lm}(\nu',\boldsymbol{\rho})\rangle_E \\
&\quad=J^l_2(x)\;\delta_{ij}\,.
\end{aligned} \tag{A3}$$

With the present basis, corrections over the external region can be performed analytically, which is not true with the shifted Gaussian functions, where integration over the relative coordinate must be done numerically [18].

[1] I. Tanihata, J. Phys. G **22**, 157 (1996).
[2] K. Riisager, Rev. Mod. Phys. **66**, 1105 (1994).
[3] M.J.G. Borge, L. Johannsen, B. Jonson, T. Nilsson, G. Nyman, K. Riisager, O. Tengblad, and K. Wilhelmsen Rolander, Nucl. Phys. **A560**, 664 (1993).
[4] I. Tanihata, H. Hamagaki, O. Hashimoto, Y. Shida, N. Yoshikawa, K. Sugimoto, O. Yamakawa, T. Kobayashi, and N. Takahashi, Phys. Rev. Lett. **55**, 2676 (1985); I. Tanihata, D. Hirata, T. Kobayashi, S. Shimoura, K. Sugimoto, and H. Toki, Phys. Lett. B **289**, 261 (1992).
[5] P.G. Hansen and B. Jonson, Europhys. Lett. **4**, 409 (1987).
[6] A. Csótó, Phys. Rev. C **48**, 165 (1993).
[7] K. Varga, Y. Suzuki, and R.G. Lovas, Nucl. Phys. **A571**, 447 (1994).
[8] K. Varga, Y. Suzuki, and Y. Ohbayasi, Phys. Rev. C **50**, 189 (1994).
[9] K. Varga and Y. Suzuki, Phys. Rev. C **52**, 2885 (1995).
[10] D. Baye, L. Desorgher, D. Guillain, and D. Herschkowitz, Phys. Rev. C **54**, 2563 (1996).
[11] G.M. Ter-Akopian, A.M. Rodin, A.S. Fomichev, S.I. Sidorchuk, S.V. Stepantsov, R. Wolski, M.L. Chelnokov, V.A. Gorshkov, A.Y. Lavrentev, V.I. Zagrebaev, and Y.T. Oganessian, Phys. Lett. B **426**, 251 (1998).
[12] R. Raabe, A. Andreyev, D. Baye, W. Bradfield-Smith, S. Cherubini, T. Davinson, P. Descouvemont, A. Di Pietro, W. Galster, M. Huyse, A.M. Laird, J. McKenzie, W.F. Mueller, A. Ostrowski, A. Piechaczek, A. Shotter, P. Van Duppen, and A. Wöhr, Phys. Lett. B (submitted).
[13] N. Soić, S. Blagus, M. Bogovac, S. Fazinić, M. Lattuada, M. Milin, D. Miljanić, D. Rendić, C. Spilateri, T. Tadić, and M. Zadro, Europhys. Lett. **34**, 7 (1996).
[14] K. Wildermuth and Y.C. Tang, *A Unified Theory of the Nucleus* (Vieweg, Braunschweig, 1977).
[15] Y.C. Tang, in *Topics in Nuclear Physics* II, Lecture Notes in

Physics (Springer, Berlin, 1981), Vol. 145, p. 572.
[16] P. Descouvemont, Phys. Rev. C **44**, 306 (1991); **47**, 210 (1993).
[17] M. Dufour, P. Descouvemont, and D. Baye, Phys. Rev. C **50**, 795 (1994).
[18] D. Baye, P.-H. Heenen, and M. Libert-Heinemann, Nucl. Phys. **A291**, 230 (1977).
[19] D. Baye and P. Descouvemont, *Proceedings of the Sapporo International Symposium on Developments of Nuclear Cluster Dynamics*, Sapporo, Japan, 1988, edited by Y. Akaishi *et al.* (World Scientific, Singapore, 1989), p. 6.
[20] K. Varga, Y. Suzuki, and I. Tanihata, Phys. Rev. C **52**, 3013 (1995).
[21] M. Kamimura, Prog. Theor. Phys. Suppl. **62**, 236 (1977).
[22] Y.C. Tang, M. LeMere, and D.R. Thompson, Phys. Rep. **47C**, 167 (1978).
[23] K. Arai, Y. Suzuki, and K. Varga, Phys. Rev. C **51**, 2488 (1995).
[24] Y. Ogawa, K. Arai, Y. Suzuki, and K. Varga, Phys. Rev. C (submitted).
[25] D. Baye and P. Descouvemont, Nucl. Phys. **A407**, 77 (1983).
[26] F. Ajzenberg-Selove, Nucl. Phys. **A490**, 1 (1988).
[27] J. Hiura and R. Tamagaki, Prog. Theor. Phys. Suppl. **52**, 25 (1972).
[28] P. Descouvemont and D. Baye, Phys. Rev. C **31**, 2274 (1985).
[29] T. Matsuse, M. Kamimura, and Y. Fukushima, Prog. Theor. Phys. **53**, 706 (1975).
[30] M. Bouten, M.-C. Bouten, H. Depuydt, and L. Schotsmans, Nucl. Phys. **A158**, 561 (1970).
[31] S. Hamada, H. Yasue, S. Kubono, M.H. Tanaka, and R.J. Peterson, Phys. Rev. C **49**, 3192 (1994).